Spectrum of Engineering Sciences
ISSN (e) 3007-3138 (p) 3007-312X Volume 4, Issue 4, 2026

REMOTE SENSING-BASED SPATIO-TEMPORAL ANALYSIS OF LAND USE LAND COVER CHANGES AND THEIR IMPACT ON LAND SURFACE TEMPERATURE AND URBAN HEAT ISLAND FORMATION OVER KARACHI

Abdur Rahman[1], Owais Khan[*2], Aniqa Murtaza[3], Ayesha Noor[4], Abuzar Khan[5], Siddique Ullah[6]

[1,2]*Department of Civil Engineering, COMSATS University Islamabad (CUI), Abbottabad Campus, Abbottabad 22060, Pakistan*
[3,4]*School of Civil and Environmental Engineering (SCEE), NUST Institute of Civil Engineering (NICE), National University of Sciences and Technology (NUST), Sector H-12, Islamabad 44000, Pakistan*
[5]*Dipartimento di Scienze della Terra, Università di Camerino, I-62032 Camerino, Italy*
[6]*Department of Environmental Sciences, COMSATS University Islamabad (CUI), Abbottabad Campus, Abbottabad 22060, Pakistan*

[1]engr.abdul141@gmail.com, [*2]engrowais082@gmail.com, [3]aniqamurtaza.ce@outlook.com, [4]ayesha4522@gmail.com, [5]abuzarkhan44@gmail.com, [6]siddiqullah142@gmail.com

DOI: https://doi.org/10.5281/zenodo.19689568

Keywords
Land Use Land Cover; Land Surface Temperature; Urban Heat Island; Remote Sensing; Cellular Automata; Karachi; Landsat; CA-Logistic Model.

Article History
Received: 26 February 2026
Accepted: 05 March 2026
Published: 22 April 2026

Corresponding Author: *
Owais Khan

Abstract

Rapid urbanisation has emerged as one of the principal drivers of Land Use Land Cover (LULC) change in developing countries, with direct consequences for Land Surface Temperature (LST) and the formation of Urban Heat Islands (UHIs). Karachi, the largest and most populous city of Pakistan, has experienced an uncontrolled built-up expansion over the past three decades owing to economic migration and natural population growth. The present study investigates the spatio-temporal dynamics of LULC and LST in Karachi during the period 1990–2020 and forecasts LULC changes for 2030, 2040 and 2050 using a Cellular Automata (CA) Logistic model. Multi-temporal Landsat 5-TM, Landsat 7-ETM+ and Landsat 8-OLI satellite images were classified into four LULC classes (built-up, vegetation, barren land, water bodies) using the Support Vector Machine (SVM) algorithm. LST was retrieved from the thermal bands and classified into five temperature zones. Results indicate that the built-up area expanded by approximately 146.86% (from 310.23 km² to 765.79 km²), while vegetation, barren land and water bodies declined by 33.3%, 7.5% and 52.0% respectively between 1990 and 2020. The area above 30 °C increased from 2.79% to 13.96%, representing a net change of +400.4%. The highest mean LST was observed over built-up surfaces, followed by barren land, vegetation and water bodies. Simulation results indicate that the built-up fraction could reach 22.7%, 24.2% and 25.5% of the total area by 2030, 2040 and 2050 respectively. The overall classification accuracy exceeded 90% for all years with Kappa coefficients ranging from 0.79 to 0.86. The findings provide a quantitative basis for urban planning, sustainable land management and UHI mitigation strategies in Karachi and can be replicated for other rapidly urbanising cities of Pakistan.

1. Introduction

Land Use Land Cover (LULC) change represents one of the most pervasive anthropogenic transformations of the Earth's surface and has been recognised as an essential component of global environmental change. LULC dynamics arise from a combination of natural processes such as flooding, earthquakes and erosion and anthropogenic forces such as urbanisation, agricultural expansion, deforestation and climatic variability. In rapidly developing countries, the scale and pace of these changes far exceed the capacity of traditional planning instruments to anticipate and manage their consequences.

Pakistan has experienced substantial LULC change over the last three decades, with long-term and short-term implications that include urban sprawl, traffic congestion, declining air and water quality, loss of vegetation cover and loss of productive agricultural land. Karachi, the economic capital of Pakistan and the largest city in the country, has witnessed one of the most intense urban transformations in South Asia. The population of Karachi rose from approximately 1 million in 1950 to over 16.5 million by 2017, driven primarily by inflow from other regions of Pakistan, migration of Afghan refugees and rural-to-urban mobility in search of employment. The resulting built-up expansion has converted large tracts of barren and vegetated land into impervious surfaces, with direct thermal consequences.

1.1 LULC and its Dynamics

Land cover refers to the physical material present at the surface of the Earth (e.g. vegetation, bare soil, water, impervious surfaces) while land use refers to the functional use to which that cover is put by human activity. Changes in LULC are driven by the interaction of biophysical and socio-economic forces and have been shown to alter the surface energy balance, water cycle, biodiversity and carbon budget. In urban contexts, the conversion of vegetated and barren surfaces to built-up material has well-documented effects on runoff, infiltration and, most importantly for the present study, on the thermal regime of the surface.

1.2 Land Surface Temperature (LST) and its Dynamics

Land Surface Temperature (LST) is defined as the radiative skin temperature of the ground and is governed by the balance between incoming shortwave radiation, outgoing longwave radiation, evapotranspiration and sensible heat exchange. LST is a key variable in climatology, hydrology and urban studies because it captures the thermal response of the surface to both meteorological forcing and land cover characteristics. Satellite-derived LST has been used since the 1970s to quantify urban warming, characterise the Urban Heat Island (UHI) phenomenon, and monitor land degradation at regional scale.

1.3 Formation of the Urban Heat Island (UHI)

The Urban Heat Island is the phenomenon in which urban areas exhibit systematically higher temperatures than their surrounding rural hinterlands. Two principal forms are recognised: the Atmospheric Urban Heat Island (AUHI), measured in the air above the surface, and the Surface Urban Heat Island (SUHI), detected from thermal remote sensing of the surface itself. Key drivers of UHI formation include the low albedo and high thermal admittance of urban construction materials, the loss of evapotranspiring vegetation, anthropogenic heat release and the geometry of the urban canopy. The UHI has important public-health implications during summer heatwaves and has been linked to increased mortality, heat stress and energy demand for cooling.

1.4 Impact of LULC Changes on LST and UHI Formation

Numerous studies have demonstrated a strong coupling between LULC and LST. Conversion of vegetated or barren surfaces to built-up cover reduces evapotranspiration, alters thermal inertia and generally raises local LST. Conversely, vegetation and water bodies act as cooling surfaces due to evapotranspiration and high specific heat capacity. Quantifying these relationships for individual cities is critical to inform urban greening strategies, zoning regulation and climate adaptation planning.

1.5 GIS and Remote Sensing Applications for LULC and LST Assessment

Remote sensing data, particularly from the Landsat series, has become the dominant data source for long-term LULC and LST analysis owing to its free availability, moderate spatial resolution (30 m) and continuous multi-decadal record. Geographic Information Systems (GIS) provide the analytical environment in which classified imagery and thermal products can be integrated with ancillary data such as topography, population and transport infrastructure. Together, remote sensing and GIS enable the reconstruction of past LULC trajectories and the projection of future trends through hybrid statistical–geospatial models.

1.6 Simulation and Prediction of Future LULC Changes

Several modelling frameworks have been proposed to simulate future LULC trajectories, including Cellular Automata (CA), Markov Chain, Artificial Neural Networks (ANN) and hybrid CA–ANN and CA–Markov approaches. CA-based models are particularly suitable for simulating spatially explicit urban growth because they represent the surface as a lattice of cells whose states evolve according to transition rules informed by driving variables such as elevation, slope, distance to roads and population density. In the present study, the CA-Logistic model, implemented in the QGIS MOLUSCE plug-in, is used to forecast LULC for 2030, 2040 and 2050.

1.7 Statement of the Problem

Karachi has received comparatively less attention in the peer-reviewed LULC–LST literature than cities of comparable size in India, China or the Middle East, despite being one of the fastest-growing coastal megacities in the world. The absence of systematic long-term quantification of its urban expansion and associated thermal response leaves a gap in the evidence base needed for local planning. Moreover, there is no publicly available projection of Karachi's LULC at decadal intervals to 2050 that is grounded in validated Landsat-derived classifications.

1.8 Objectives

The present study is guided by three specific objectives:

(i) to quantify and map LULC change in Karachi for the period 1990–2020 using multi-temporal Landsat data;

(ii) to retrieve LST from Landsat thermal bands, classify it into five temperature zones and examine its variation across LULC classes; and

(iii) to simulate and forecast LULC for 2030, 2040 and 2050 using a CA-Logistic model, and to discuss the implications for UHI mitigation and sustainable urban planning in Karachi.

2. Literature Review

2.1 LULC Dynamics

The study of LULC dynamics has produced a large body of literature employing remote sensing and GIS. Fazal combined aerial photography and satellite imagery with field surveys to quantify urban expansion in Saharanpur, India, between 1988 and 1998, and reported that 5% of agricultural land was converted to built-up cover driven by population growth and in-migration. Mundia and Aniya used three Landsat images to analyse LULC in Nairobi for 1976–2000 and observed a 47 km² expansion of built-up cover at the expense of forest, with economic growth and accessibility identified as the principal drivers. Fan et al. examined Guangzhou, China, for 1979–2003 and found that the urban area expanded from 141.15 km² to 437.70 km², shifting from a compact to a leapfrogging pattern along the major road corridors. These studies collectively demonstrate that urbanisation is the dominant force re-shaping LULC in developing-country cities and that its spatial pattern is conditioned strongly by transport infrastructure.

2.2 Land Surface Temperature (LST) Dynamics

LST is a critical parameter in research on ocean circulation, climate variability, weather forecasting and surface–atmosphere energy exchange. Mujabar analysed the LST of Jubail Industrial City, Saudi Arabia, and reported that January LST ranged from 20 to 30 °C, rising gradually through March and peaking in June. Summer LST in residential zones reached 40–50

°C, while values of 50–55 °C were recorded in the industrial district and exceeded 60 °C near the iron and steel mills. Jafari et al. investigated LST and green-space configuration in Neyshabur, Iran, using Landsat ETM+ imagery and five landscape metrics (LSI, MPFD, ED, MPS, MSI). Their findings showed that the spatial arrangement of green space significantly influenced LST and UHI intensity, with LSI exerting the strongest effect and ED the weakest.

2.3 Urban Heat Island (UHI)

The UHI phenomenon refers to the elevated surface or air temperatures observed in urban areas relative to their surroundings. UHIs generally dissipate with distance from the urban core; their magnitude and shape are modulated by climate zone, regional setting and the city's specific LULC composition. Because urban fabric tends to be darker, drier and more thermally massive than natural cover, cities create closed isotherms of elevated temperature that persist during both day and night. The peculiarities of each city's LULC exert a substantial influence on UHI formation and intensity.

2.4 The Effects of LULC Changes on LST

The coupling between LULC change and LST has been extensively documented. Fathian et al. used the Temperature-Vegetation Index to study the eastern sub-basins of Urmia Lake, Iran, and found that agricultural activity was responsible for most LST change between 1989 and 2002. Ullah et al. examined six districts of Xi'an, China, from 1987 to 2018 and recorded a 69.6% increase in urban area with a sharp decline in peri-urban vegetation cover; a significantly negative LST–NDVI relationship was observed, implying that vegetation can partially offset the thermal impact of urbanisation. In Pakistan's lower Himalayan region, Ullah et al. used Landsat data, SVM classification and a combined CA–ANN model to project that built-up area would increase by 2.27% by 2032 and 4.13% by 2047, pushing the fraction of the study area with LST > 27 °C from 26% in 2017 to 42% in 2032 and 60% in 2047. Akbar et al. similarly reported, for the same region, that the built-up fraction could rise from 11% in 2017 to 12.48% in 2032 and 14.65% in 2047, with the area above 30 °C expanding from 18.64% to 58.02% over the same horizon.

2.5 Data and Techniques Used for LULC and LST Classification

In most developing countries, ground survey has traditionally been the principal method of monitoring urban land use. Because ground survey is costly and time-consuming, aerial photography and satellite data have become the standard alternative. Four categories of LULC change detection are recognised: (i) recognition of the nature of change; (ii) detection of changes that have occurred; (iii) determination of the areal extent of change; and (iv) assessment of the spatial pattern of change. Since 1970, LST has been studied using thermal infrared (TIR) remote sensing from a progression of satellite sensors operating at varying spatial resolutions. Rahman et al. used Landsat TM to investigate the relationship between LST, NDVI and impervious surfaces, while Ullah et al. combined Landsat TM, ETM+ and OLI data to simulate LULC and its impact on LST in the lower Himalayan region.

2.6 Simulation and Prediction of Future LULC Changes

Land-use models are useful both for diagnosing the drivers of change and for informing land-use conservation. Khawaldah et al. applied a CA–Markov model to Irbid, Jordan, and projected that the built-up area, which had increased by 386.9% between 1984 and 2018, would grow by a further 19.5% and 64.6% by 2030 and 2050 respectively. Mansour et al. studied Nizwa, Oman, and forecast 12,014 ha of net urban growth by 2028 using CA–Markov. Hadi et al. modelled LULC for Tikrit, Iraq, between 2010 and 2030 and reported a significant projected decrease in vegetation (45.11 km²) accompanied by an increase in urban area (58.42 km²). Collectively, these studies confirm the utility of CA-based frameworks for decadal LULC projection and motivate their application in the present analysis of Karachi.

3. Research Methodology

3.1 Study Area

Karachi is the largest economic centre of Pakistan, located on the south-eastern coastline

of Sindh Province along the Arabian Sea. Administratively it comprises five districts: Karachi Central, Karachi East, Karachi West, Karachi South and Malir. The total area of the city is approximately 3,780 km² and the population, according to the United Nations World Population Prospects, exceeds 16.5 million. The climate is classified as tropical, characterised by mild winters and hot summers, with a mean annual temperature of 26.1 °C and a total annual rainfall of 174.6 mm. The population of the city rose from approximately 1 million in 1950 to its present level, primarily because of economic migration from other regions of Pakistan. This demographic surge has driven the unplanned expansion of built-up land and is associated with rising LST, increased flood frequency and periodic heat-stress events. The location of the study area is shown in Figure 1.

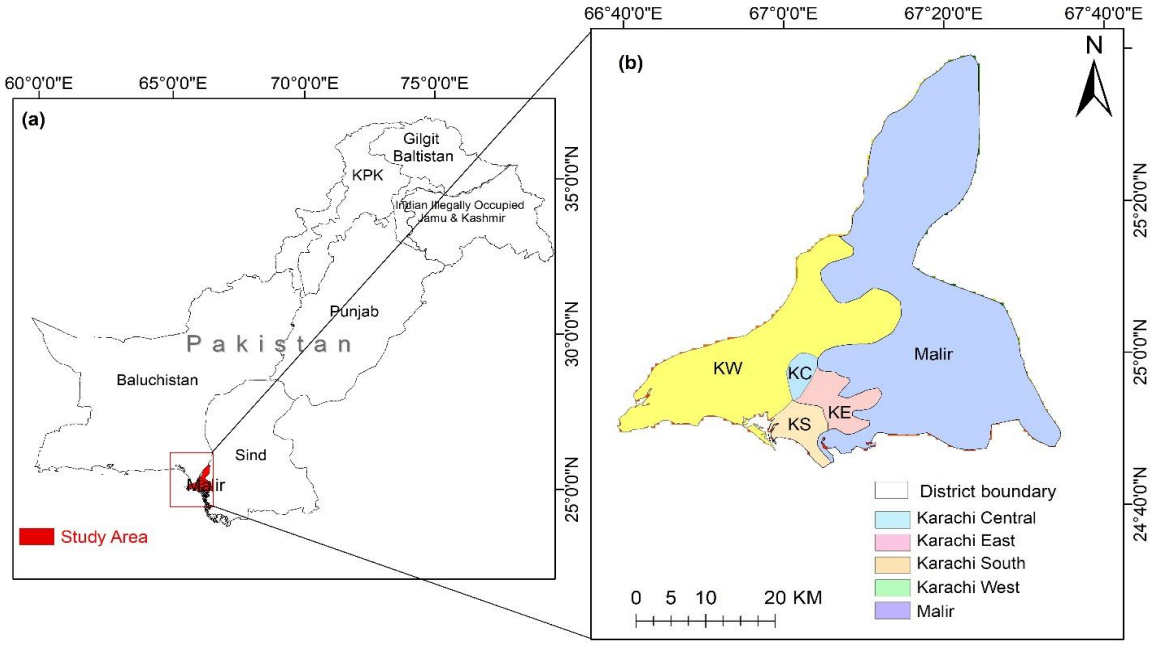

Figure 1. (a) Location of the study area (Karachi) within Pakistan; and (b) administrative districts of the study area (KC – Karachi Central, KE – Karachi East, KS – Karachi South, KW – Karachi West, Malir).

3.2 Data Sets

Landsat satellite data for the years 1990, 2000, 2010 and 2020 were used in this study. Images were downloaded from the United States Geological Survey (USGS) Earth Explorer portal (https://earthexplorer.usgs.gov/). Three Landsat sensors were employed, namely Landsat 5-TM, Landsat 7-ETM+ and Landsat 8-OLI, covering a 30-year period at approximately decadal intervals. The study area spans two Landsat tiles (path/row 152/42 and 152/43), both of which were downloaded on each acquisition date, mosaicked and subsequently clipped to the administrative boundary of Karachi. Prior to download, a cloud-cover threshold of less than 2% was enforced to ensure image clarity. Details of the Landsat data are summarised in Table 1.

Table 1. Landsat satellite data used for LULC and LST analysis (1990–2020).

Date	Scene IDs	Sensor	Cloud Cover (%)	Path / Row
24 May 1990	LT51520421990144RSA00; LT51520431990144RSA00	Landsat 5 TM	< 2	152/42; 152/43

Date	Scene IDs	Sensor	Cloud Cover (%)	Path / Row
25 April 2000	LE71520422000116SGS00; LE71520432000116SGS00	Landsat 7 ETM+	< 2	152/42; 152/43
16 June 2010	LT51520422010167KHC00; LT51520432010167KHC00	Landsat 5 TM	< 2	152/42; 152/43
10 May 2020	LC81520422020131LGN00; LC81520432020131LGN00	Landsat 8 OLI	< 2	152/42; 152/43

3.3 Methods and Data Processing

The methodology of the study comprises six sequential steps: (i) pre-treatment of the Landsat datasets; (ii) LULC classification and accuracy assessment; (iii) LST estimation; (iv) classification of temperature zones; (v) establishment of the relationship between LULC and LST using zonal statistics; and (vi) simulation of future LULC for 2030, 2040 and 2050 using a CA-Logistic model. A schematic of the methodological workflow is presented in Figure 2.

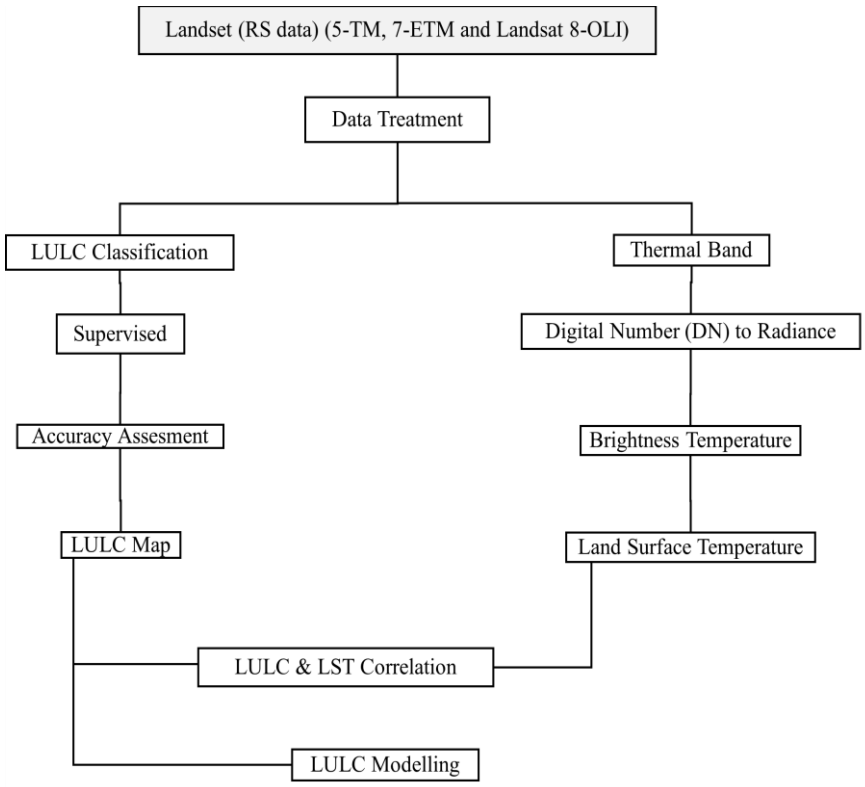

Figure 2. Methodological flow-chart for LULC estimation, LST retrieval, LULC–LST correlation and LULC forecasting.

3.3.1 Pre-treatment of Datasets

Raw Landsat scenes were pre-processed using the Semi-automatic Classification Plug-in (SCP) in QGIS. Pre-treatment comprised radiometric calibration, atmospheric correction and, for Landsat 7-ETM+ acquisitions after 2003, gap-filling to compensate for the Scan Line Corrector (SLC-off) failure. Atmospheric correction removes the attenuating effect of the atmosphere so that image pixel values correspond to surface reflectance, while radiometric correction reduces sensor-related

errors in the raw digital numbers. Both tiles covering the study area were processed independently and subsequently mosaicked.

3.3.2 LULC Classification and Accuracy Assessment

Supervised classification was carried out in ENVI 5.3 using the Support Vector Machine (SVM) algorithm. SVM is a non-parametric classifier that builds an optimal separating hyper-plane in feature space and generally outperforms maximum-likelihood classifiers on heterogeneous urban imagery. Four LULC classes were defined following the Anderson classification scheme: built-up, barren land, vegetation and water bodies (Table 2). Training samples were drawn from high-resolution reference imagery for each date. Accuracy was evaluated through a confusion matrix using 200 randomly generated reference pixels per classified image, from which user's accuracy, producer's accuracy, overall accuracy and the Kappa coefficient were computed.

Table 2. LULC classes selected for classification based on the Anderson classification scheme.

LULC Class	Description
Built-up	Residential land, industrial land, commercial land, metalled roads and all other impervious constructed surfaces.
Barren land	Area covered by barren rock, sand and exposed soil with little or no vegetation cover.
Vegetation	Forest, shrubland, grassland and agricultural land.
Water body	Area covered by lakes, rivers, drainages, coastal creeks and other permanent surface water.

3.3.3 Land Surface Temperature (LST) Estimation

The thermal band(s) of each Landsat sensor were used to retrieve LST. Band 6 was used for Landsat 5-TM and Landsat 7-ETM+, while band 10 and band 11 were used for Landsat 8-OLI (the LST from the two OLI thermal bands was averaged). The retrieval procedure comprises four sequential steps, which are summarised below.

3.3.3.1 Conversion of Digital Numbers to Radiance

The raw digital numbers (DN) stored in the thermal band were first converted to at-sensor spectral radiance using Eq. (1):

$$L\_\lambda = ((L\_max - L\_min) / 255) \times DN + L\_min \quad (1)$$

where L_λ is the spectral radiance at the sensor ($W \cdot m^{-2} \cdot sr^{-1} \cdot \mu m^{-1}$); L_max and L_min are the maximum and minimum radiances obtained from the scene metadata; and DN is the raw digital number.

3.3.3.2 Conversion of Radiance to Brightness Temperature

The spectral radiance was then converted to at-sensor brightness temperature (T_B) using the calibration constants K_1 and K_2 specific to each sensor, as given in Eq. (2):

$$T\_B = K_2 / \ln((K_1 / L\_\lambda) + 1) - 273.15 \quad (2)$$

where T_B is the brightness temperature (K); K_1 and K_2 are the calibration constants read from the scene metadata; and L_λ is the spectral radiance computed in Eq. (1).

3.3.3.3 Conversion from Kelvin to Celsius

Brightness temperature values in Kelvin were converted to degrees Celsius using Eq. (3):

$$T\_B\ (°C) = T\_B\ (K) - 273.15 \quad (3)$$

3.3.3.4 Conversion of Brightness Temperature to LST

The brightness temperature was corrected for surface emissivity (ε) to obtain LST using Eq. (4):

$$LST = T\_B / (1 + (\lambda \times T\_B / \rho) \times \ln(\varepsilon)) \quad (4)$$

where λ is the wavelength of the emitted radiation (≈ 11.5 μm for Landsat TM/ETM+ band 6); $\rho = h \cdot c / \sigma = 1.4388 \times 10^{-2}$ m·K; h is Planck's constant (6.626×10^{-34} J·s); σ is

Boltzmann's constant (1.38×10^{-23} J/K); c is the speed of light (2.998×10^{8} m/s); and ε is the land surface emissivity.

Land surface emissivity was estimated from the Proportion of Vegetation (PV), which was in turn derived from the Normalised Difference Vegetation Index (NDVI) using Eqs. (5) and (6):

$$PV = [\,(NDVI - NDVI\_min) / (NDVI\_max - NDVI\_min)\,]^2 \quad (5)$$

$$\varepsilon = 0.004 \times PV + 0.986 \quad (6)$$

3.3.3.5 Normalisation of LST

To make LST values comparable across acquisition years (which differ in sensor, season and atmospheric conditions), the retrieved LST images were standardised using Eq. (7) following Ullah et al.:

$$LST\_nj = ((LST\_j - \overline{LST\_j}) / \sigma\_j) \times \sigma\_i + \overline{LST\_i} \quad (7)$$

where LST_nj is the pixel-specific normalised LST for year j (1990, 2000 or 2010); LST_j is the original pixel value before normalisation; $\overline{LST\_j}$ and σ_j are the mean and standard deviation of the LST image for year j; and $\overline{LST\_i}$ and σ_i are the mean and standard deviation of the reference image (year 2020).

3.4 Classification of Temperature Zones

The normalised LST values were classified into five temperature zones: (i) < 18 °C; (ii) 18 – < 22 °C; (iii) 22 – < 26 °C; (iv) 26 – < 30 °C; and (v) > 30 °C. The same class breaks were applied to all four acquisition years to enable consistent comparison of the areal distribution of temperature zones through time.

3.5 Relationship between LULC and LST

Zonal statistics were computed in ArcGIS 10.2 to determine the mean LST within each LULC class for each acquisition year. This enabled the construction of a time series of mean LST by LULC class, which was used to quantify the thermal signature of each cover type and to estimate the sensitivity of LST to urbanisation.

3.6 Simulating LULC Changes for 2030, 2040 and 2050

LULC for 2030, 2040 and 2050 was simulated using a Cellular Automata Logistic (CA-Logistic) model implemented in the MOLUSCE plug-in of QGIS. The CA-Logistic model requires a pair of classified images spanning a historical training interval and a set of driving variables. For this study, the 2010 and 2020 classified images were used as the training pair, and four driving variables were incorporated: elevation, slope, population density and Euclidean distance from the main road network. Elevation and slope were derived from the Shuttle Radar Topography Mission (SRTM) Digital Elevation Model (DEM). A transition-potential matrix was first extracted from the training images and then applied iteratively at decadal intervals to generate 2030, 2040 and 2050 LULC maps.

Model performance was validated by comparing the simulated 2020 LULC map against the observed 2020 classification. Validation metrics generated by the MOLUSCE plug-in include the K-location, K-histogram, overall Kappa coefficient and percent correctness. These metrics collectively assess whether the model reproduces both the quantity and the spatial allocation of each LULC class.

4. Results and Discussion

This section presents the results of the LULC classification and LST retrieval for 1990–2020, an assessment of classification accuracy, the analysis of LULC–LST relationships and the CA-Logistic projections for 2030, 2040 and 2050. The results are interpreted in light of the published literature on urban dynamics in comparable cities.

4.1 Quantification and Mapping of LULC (1990–2020)

Figure 3 presents the classified LULC maps and corresponding compositional pie-charts for 1990, 2000, 2010 and 2020, while Table 3 summarises the areas covered by each class. In 1990, barren land dominated the study area (2,599.5 km²; ≈ 72.6% of the total), followed by vegetation (474.3 km² ≈ 13.3%), built-up land (310.23 km² ≈ 8.7%) and water bodies (195.43 km² ≈ 5.5%). The northern and north-eastern portions of Karachi, which are further from the coast, were dominated by barren land, whereas the existing urban footprint was concentrated in the south along the Arabian Sea (Figure 3a).

By 2000, the built-up class had expanded to 459.04 km² (12.8%) while vegetation fell to 436.12 km² and barren land to 2,532.92 km².

The expansion is visible in Figure 3b, most markedly in the centre of the study area. The 2010 map (Figure 3c) shows further intensification of the urban core, with built-up area rising to 602.35 km² (16.8%). By 2020 (Figure 3d), the built-up class had reached 765.79 km² (21.4%), while vegetation and water bodies had declined to 316.40 km² and 93.81 km² respectively. The progressive expansion of the built-up core toward the north-west and east, at the expense of both barren land and peripheral vegetation, is consistent with reports of unplanned urban growth driven by economic migration and informal settlement. Comparable patterns have been documented for Nairobi (1976–2003) and for Guangzhou (1979–2003).

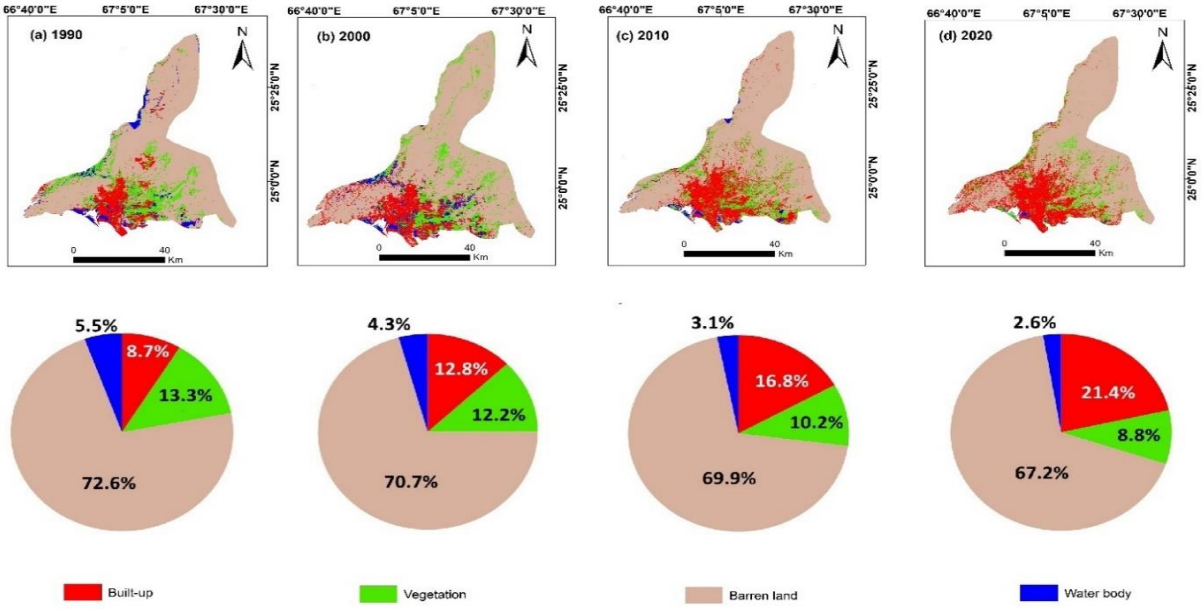

Figure 3. LULC maps and compositional pie-charts of the study area for (a) 1990; (b) 2000; (c) 2010; and (d) 2020.

4.2 Trends and Rate of Change of LULC (1990–2020)

Table 3 quantifies the changes in each LULC class over the three decadal intervals 1990–2000, 2000–2010 and 2010–2020, as well as the net change for the full data period. The built-up class exhibited a monotonic increasing trend throughout, with the largest decadal gain (+163.44 km²) occurring in the final interval (2010–2020). The net change in built-up cover over 1990–2020 was +455.56 km², equivalent to an approximately 147% relative increase on the 1990 baseline. Vegetation declined continuously, losing a total of 157.9 km² (≈ 33.3% of its 1990 area), with the largest decadal loss (−69.93 km²) recorded during 2000–2010. Barren land lost 194.79 km² (≈ 7.5%), and water bodies declined by 101.62 km² (≈ 52.0%), the latter reflecting reclamation, siltation of coastal creeks and loss of small inland drainages.

The systematic conversion of vegetation to built-up cover is consistent with published findings from other Pakistani cities (for example Lahore, 1988–2016) and from cities of comparable size elsewhere in the Global South. Vegetation in Karachi tends to occupy low-lying, relatively flat ground close to existing residential zones, which makes it particularly vulnerable to settlement conversion.

Table 3. LULC changes in Karachi during the three decadal intervals and the overall study period (1990–2020).

LULC Class	1990 (km²)	2000 (km²)	2010 (km²)	2020 (km²)	Δ 1990–2000 (km²)	Δ 2000–2010 (km²)	Net Δ 1990–2020 (km²)
Built-up	310.23	459.04	602.35	765.79	+148.81	+143.31	+455.56
Vegetation	474.30	436.12	366.19	316.40	−38.18	−69.93	−157.90
Barren Land	2599.50	2532.92	2501.38	2404.71	−66.58	−31.54	−194.79
Water Bodies	195.43	152.63	111.00	93.81	−42.80	−41.63	−101.62

4.3 Accuracy Assessment of the Classified Images

Classification accuracy was assessed by comparing the classified LULC images against 200 reference pixels per year drawn from higher-resolution RGB composites. For each of the four years the overall accuracy exceeded 90% and the Kappa coefficient ranged between 0.79 and 0.86 (Table 4). These values fall within the range typically considered acceptable for moderate-resolution Landsat classifications and compare favourably to similar studies conducted on Lahore and on the lower Himalayan region of Pakistan.

Table 4. Accuracy assessment of the classified LULC maps for 1990, 2000, 2010 and 2020.

Year	User's Accuracy (%)	Producer's Accuracy (%)	Overall Accuracy (%)	Kappa Coefficient
1990	92.72	92.27	92.49	0.79
2000	93.51	93.05	93.28	0.86
2010	91.58	90.59	91.09	0.81
2020	92.14	91.15	91.04	0.82

4.4 Drivers of LULC Change in Karachi

The LULC transformations detected in Karachi can be attributed to a combination of demographic, socio-economic and political drivers. The principal demographic driver is sustained population growth, which combines natural increase with continuous rural-to-urban migration. Economic migration from interior Sindh, southern Punjab and Balochistan, together with the historical settlement of Afghan refugees, has contributed directly to the expansion of residential, commercial and industrial built-up cover. The industrial character of Karachi further accelerates LULC change, both directly through the conversion of land to industrial estates and indirectly by attracting labour migration. Factors secondary to urbanisation but relevant to the LULC record include changes in agricultural practice, alterations in surface hydrology and, in recent years, coastal reclamation.

4.5 Mapping and Quantification of LST (1990–2020)

The spatial distribution of LST retrieved from the Landsat thermal bands for 1990, 2000, 2010 and 2020 is shown in Figure 4, and the areal distribution of temperature zones is given in Table 5. The mean LST of the study area was 32.12 ± 3.1 °C in 1990, rising to 35.11 ± 3.29 °C in 2000, falling to 31.01 ± 3.29 °C in 2010, and reaching 35.12 ± 3.86 °C by 2020. In 1990 the dominant LST zone was 26 – < 30 °C (76.2%), followed by 22 – < 26 °C (14.3%); the > 30 °C zone covered only 2.8% of the study area. By 2020 the > 30 °C zone had expanded to

13.96% and was concentrated over the north-eastern barren land and the high-density built-up districts. The cooler zones (< 18 °C, 18 – < 22 °C and 22 – < 26 °C) contracted progressively across all four years, most markedly over the coastal belt in the south-west where the sea breeze continues to moderate surface temperature.

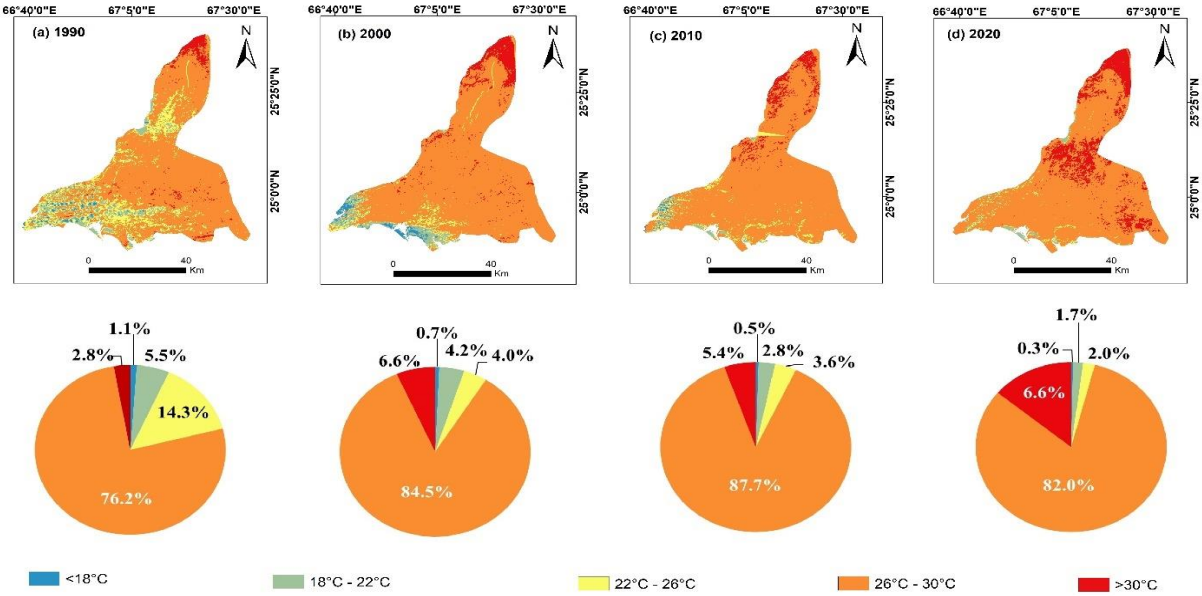

Figure 4. Land Surface Temperature (LST) maps and areal pie-charts of the study area for (a) 1990; (b) 2000; (c) 2010; and (d) 2020.

4.6 Net Change and Trends in LST during 1990–2020

The trend analysis summarised in Table 5 indicates that the three lower LST zones (< 18, 18 – < 22 and 22 – < 26 °C) all declined monotonically. The largest net contraction was recorded for the 22 – < 26 °C zone, with a net change of −441.4 km² over 1990–2020. The 26 – < 30 °C zone expanded by +206.9 km² net, while the > 30 °C zone exhibited the largest relative increase, with a net gain of +399.9 km² (equivalent to a roughly fivefold expansion on its 1990 area). The expansion of the highest temperature zone is most pronounced in the final decade (2010–2020), during which it grew by +307.9 km². These results confirm a clear upward shift in the thermal distribution of Karachi that is synchronous with the documented expansion of built-up area. Comparable trends have been reported elsewhere; for example, Weng et al. attributed a 13.01 K increase in surface radiant temperature in the urbanised Zhujiang Delta to LULC transformation.

Table 5. LST-zone area changes during the three decadal intervals and the overall study period (1990–2020).

LST Class	1990 (km²)	2000 (km²)	2010 (km²)	2020 (km²)	Δ 1990–2000	Δ 2010–2020	Net Δ 1990–2020
< 18 °C	40.10	25.10	16.80	12.20	−15.00	−4.70	−27.90
18 – < 22 °C	198.00	151.40	100.20	60.50	−46.50	−39.70	−137.50
22 – < 26 °C	511.90	142.50	130.00	70.50	−369.50	−59.40	−441.40
26 – < 30 °C	2729.40	3024.40	3141.10	2936.30	+295.00	−204.80	+206.90
> 30 °C	99.90	236.30	191.90	499.80	+136.40	+307.90	+399.90

4.7 Mean LST Variation across LULC Classes

Figure 5 displays the mean LST in each LULC class for 1990, 2000, 2010 and 2020, computed by zonal statistics. Built-up cover consistently exhibited the highest mean LST across all four years, rising from 34.23 °C in 1990 to 38.54 °C in 2020. Barren land was a close second, rising from 33.32 °C to 37.37 °C. Vegetation ranked third (30.91 °C → 35.25 °C) and water bodies fourth (28.03 °C → 31.63 °C). All four LULC classes showed a positive temperature trend, with approximate rates of change of +0.15 °C/yr for built-up, +0.13 °C/yr for barren land, +0.14 °C/yr for vegetation and +0.12 °C/yr for water bodies. The uniform warming across all classes is consistent with a regional climatic signal superimposed on the urbanisation-driven component. The thermal signature in which impervious surfaces exhibit the highest LST, followed by barren, then vegetated and water surfaces, has been repeatedly documented in studies from both developed and developing cities.

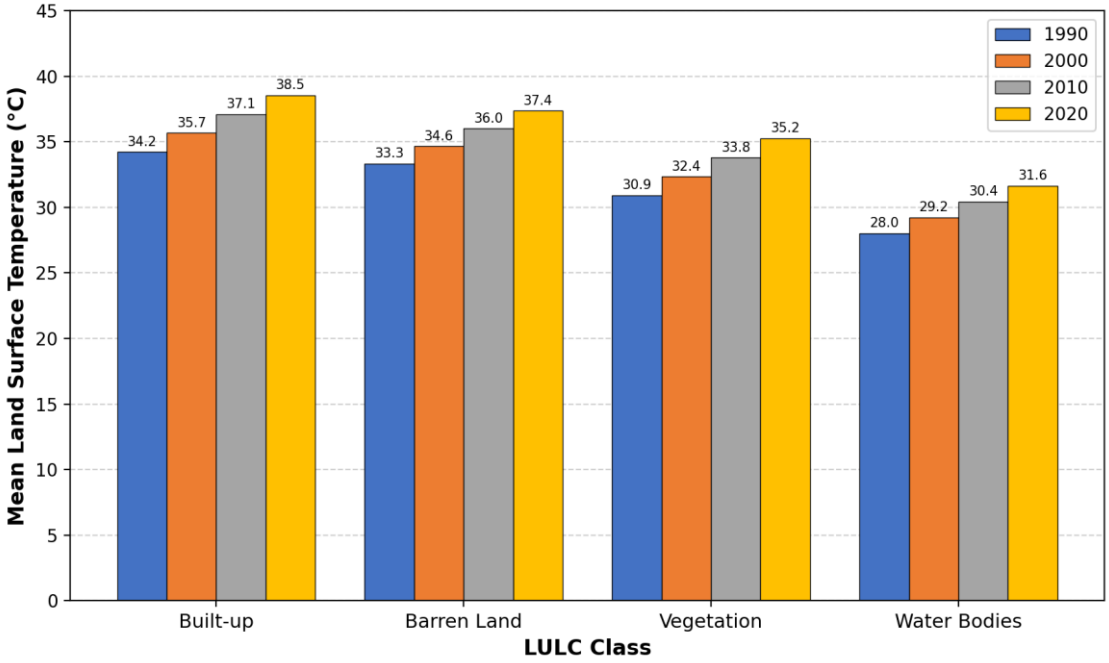

Figure 5. Mean Land Surface Temperature (LST) in different LULC classes of the study area for 1990, 2000, 2010 and 2020.

4.8 Areal Distribution Trends across LST Zones

The distribution of area under each LST zone for 1990, 2000, 2010 and 2020 is presented in Figure 6. The 22 – < 26 °C zone shrank sharply, from 14.3% of the total area in 1990 to 4.0% in 2000 and 2.0% in 2020. The 18 – < 22 °C zone also contracted steadily (5.5% → 1.7%), and the < 18 °C zone declined from 1.1% to 0.3%. The 26 – < 30 °C zone grew from 76.2% in 1990 to a peak of 87.7% in 2010, before retreating to 82.0% in 2020 as part of its area transitioned to the > 30 °C zone. The > 30 °C zone traced the clearest warming signal, rising from 2.8% in 1990 to 6.6% in 2000, falling slightly to 5.4% in 2010, and then expanding sharply to 14.0% in 2020. A similar pattern of rapid growth in the highest temperature class was reported for Xi'an (1987–2018) and for the lower Himalayan region of Pakistan (1987–2017).

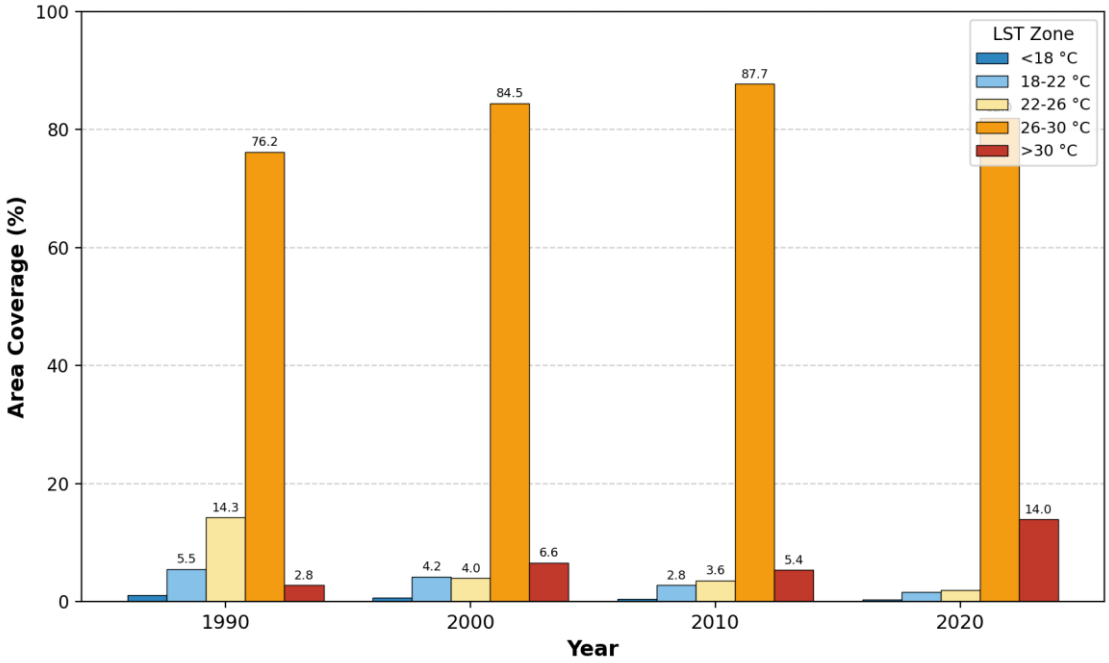

Figure 6. Areal distribution of different LST (°C) zones in the study area during 1990–2020.

4.9 Simulation of LULC Changes for 2030, 2040 and 2050

The CA-Logistic model was trained on the 2010 and 2020 classified images with elevation, slope, population density and Euclidean distance to main roads as driving variables. Validation of the model against the observed 2020 classification produced an overall Kappa coefficient and percent correctness that met the thresholds recommended in comparable published applications, confirming that the model is fit for decadal projection. The simulated LULC maps for 2030, 2040 and 2050 are presented in Figure 7 and the corresponding areal statistics are summarised in Table 6.

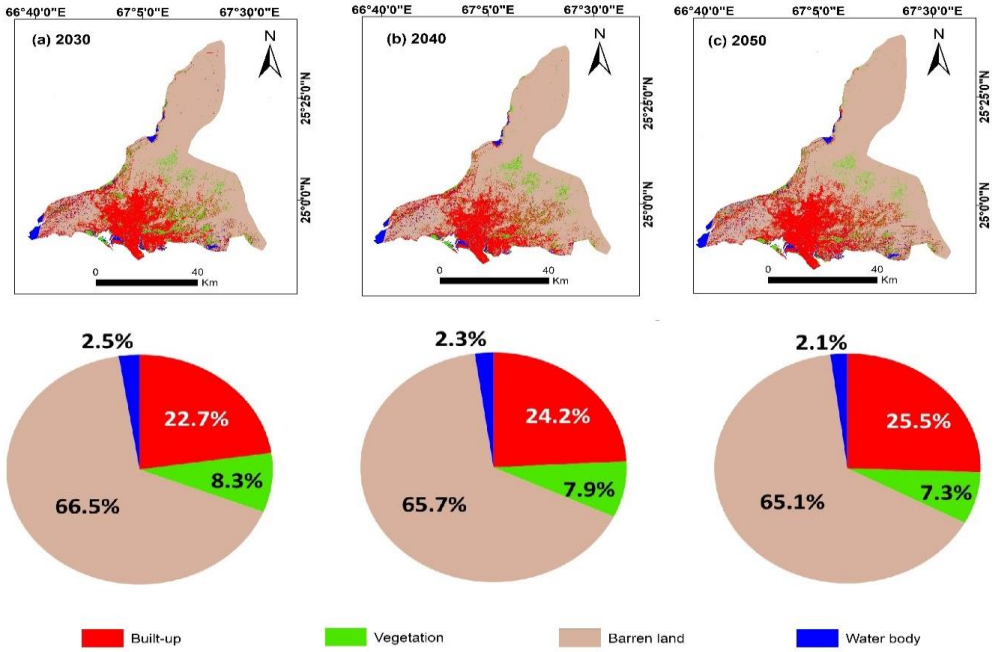

Figure 7. Simulated LULC maps and compositional pie-charts of the study area for (a) 2030; (b) 2040; and (c) 2050 produced by the CA-Logistic model.

The projections indicate that the built-up fraction will continue to expand throughout the simulation horizon, reaching 811.72 km² (22.7%) by 2030, 865.45 km² (24.2%) by 2040 and 913.54 km² (25.5%) by 2050. Decadal gains are approximately +45.93, +53.73 and +48.09 km² for the three intervals respectively, yielding a net increase of +147.75 km² between 2020 and 2050. Barren land is the class most reduced in absolute terms, declining by 74.24 km² net, followed by vegetation (−54.06 km²) and water bodies (−20.31 km²). Most of the new built-up cover is simulated to emerge through infilling of the existing urban core and expansion northward and eastward along the principal road corridors, consistent with historical growth trajectories.

Table 6. Predicted LULC changes in Karachi during the three decadal intervals and the overall forecast period (2020–2050) produced by the CA-Logistic model.

LULC Class	2020 (km²)	2030 (km²)	2040 (km²)	2050 (km²)	Δ 2020–2030 (km²)	Δ 2040–2050 (km²)	Net Δ 2020–2050 (km²)
Built-up	765.79	811.72	865.45	913.54	+45.93	+48.09	+147.75
Vegetation	316.40	298.00	282.44	262.34	−18.40	−20.10	−54.06
Barren Land	2404.71	2380.16	2351.33	2330.47	−24.55	−20.86	−74.24
Water Bodies	93.81	89.97	80.72	73.50	−3.84	−7.22	−20.31

If unaddressed, the projected expansion of built-up cover is likely to drive further warming and strengthen the SUHI. The continuation of trends observed between 1990 and 2020 implies that the > 30 °C LST zone, which already expanded by a factor of approximately five over three decades, could cover a substantially larger fraction of Karachi by 2050. This is of particular concern given the city's coastal-tropical climate and its already high summer heat stress. Comparable extrapolations have been reported for Patna, India, and for Chittagong, Bangladesh, where rapid built-up growth is associated with projected declines in vegetation cover.

5. Conclusions and Recommendations

5.1 Conclusions

This study used multi-temporal Landsat data and a CA-Logistic model to quantify LULC and LST changes in Karachi during 1990–2020 and to project LULC for 2030, 2040 and 2050. The principal findings are as follows:

(i) The classified Landsat images exhibited overall accuracies above 90% and Kappa coefficients between 0.79 and 0.86, confirming their suitability for decadal LULC and LST analysis in the study area.

(ii) Built-up area expanded from 310.23 km² in 1990 to 765.79 km² in 2020 (+146.9%), while vegetation, barren land and water bodies contracted by 33.3%, 7.5% and 52.0% respectively.

(iii) The highest mean LST was consistently observed over built-up and barren surfaces, followed by vegetation and water bodies. All four LULC classes warmed during the study period, indicating a combined regional and urbanisation-driven thermal signal.

(iv) The area within the > 30 °C LST zone expanded from 2.8% of the study area in 1990 to 14.0% in 2020, equivalent to a net change of approximately +400%.

(v) CA-Logistic projections indicate that built-up cover will continue to grow to 22.7%, 24.2% and 25.5% of the study area by 2030, 2040 and 2050 respectively, with corresponding losses of vegetation, barren land and water.

5.2 Recommendations

The findings lead to the following recommendations for planners and

policymakers in Karachi and in other rapidly urbanising cities of Pakistan:

- Urban forestry should be scaled up. Systematic plantation of trees and development of urban green corridors along arterial roads and in residential districts can attenuate the rise in LST within the urban core.
- New residential and industrial developments should be conditionally approved on the provision of on-site green cover at a specified minimum threshold, as already practised in several South Asian cities.
- Coastal wetlands and inland water bodies should be protected from reclamation, because their continued loss reduces the buffering capacity against UHI formation.
- Municipal authorities should incorporate satellite-derived LULC and LST monitoring into their routine planning cycle, since Landsat-based analysis is inexpensive and provides evidence that is directly actionable for zoning and heat-risk mapping.
- The methodology employed here can be replicated in other rapidly urbanising cities of Pakistan, including Lahore, Faisalabad, Peshawar and Quetta, to provide a nationally consistent evidence base for UHI-aware urban planning.

Acknowledgements

The authors gratefully acknowledge the United States Geological Survey (USGS) for providing free Landsat data through the Earth Explorer portal, the Department of Civil Engineering and the Department of Environmental Sciences at COMSATS University Islamabad (Abbottabad Campus) for technical support, and the QGIS MOLUSCE development team for making the CA-Logistic tool freely available.

REFERENCES

[1] Di Gregorio, A. (2005). Land cover classification system: classification concepts and user manual: LCCS (Vol. 2). Food & Agriculture Organization of the United Nations.

[2] Zhao, R., Chen, Y., Shi, P., Zhang, L., Pan, J., & Zhao, H. (2013). Land use and land cover change and driving mechanism in the arid inland river basin: a case study of Tarim River, Xinjiang, China. Environmental Earth Sciences, 68(2), 591–604.

[3] Nendel, C., Hu, Y., & Lakes, T. (2018). Land-use change and land degradation on the Mongolian Plateau from 1975 to 2015—A case study from Xilingol, China. Land Degradation & Development, 29(6), 1595–1606.

[4] Ribeiro, M. C., Martensen, A. C., Metzger, J. P., Tabarelli, M., Scarano, F., & Fortin, M. J. (2011). The Brazilian Atlantic Forest: a shrinking biodiversity hotspot. In Biodiversity Hotspots (pp. 405–434). Springer, Berlin, Heidelberg.

[5] Mather, A. S., & Needle, C. L. (2000). The relationships of population and forest trends. Geographical Journal, 166(1), 2–13.

[6] Houghton, R. A. (1994). The worldwide extent of land-use change. BioScience, 44(5), 305–313.

[7] Sun, X., Fan, D., Liu, M., Liao, H., & Tian, Y. (2019). Persistent impact of human activities on trace metals in the Yangtze River Estuary and the East China Sea: evidence from sedimentary records of the last 60 years. Science of the Total Environment, 654, 878–889.

[8] Alig, R. J., Kline, J. D., & Lichtenstein, M. (2004). Urbanization on the US landscape: looking ahead in the 21st century. Landscape and Urban Planning, 69(2–3), 219–234.

[9] Seto, K. C., Güneralp, B., & Hutyra, L. R. (2012). Global forecasts of urban expansion to 2030 and direct impacts on biodiversity and carbon pools. Proceedings of the National Academy of Sciences, 109(40), 16083–16088.

[10] Fazal, S. (2000). Urban expansion and loss of agricultural land—a GIS based study of Saharanpur City, India. Environment and Urbanization, 12(2), 133–149.

[11] Mundia, C. N., & Aniya, M. (2005). Analysis of land use/cover changes and urban expansion of Nairobi city using remote sensing and GIS. International Journal of Remote Sensing, 26(13), 2831–2849.

[12] Fan, F., Wang, Y., Qiu, M., & Wang, Z. (2009). Evaluating the temporal and spatial urban expansion patterns of Guangzhou from 1979 to 2003 by remote sensing and GIS methods. International Journal of Geographical Information Science, 23(11), 1371–1388.

[13] Mujabar, P. S. (2019). Spatial–temporal variation of land surface temperature of Jubail Industrial City, Saudi Arabia due to seasonal effect by using Thermal Infrared Remote Sensor (TIRS) satellite data. Journal of African Earth Sciences, 155, 54–63.

[14] Jafari, E., Soltanifard, H., Aliabadi, K., & Karachi, H. (2017). Assessment of the effect of Neyshabur green spatial configuration on the temperature of land surface and heat islands. Open Journal of Ecology, 7(9), 554–567.

[15] Huang, G., Zhou, W., & Cadenasso, M. L. (2011). Is everyone hot in the city? Spatial pattern of land surface temperatures, land cover and neighborhood socioeconomic characteristics in Baltimore, MD. Journal of Environmental Management, 92(7), 1753–1759.

[16] Voogt, J. A. (2004). Urban Heat Islands: Hotter Cities. American Institute of Biological Sciences.

[17] Roth, M. (2013). Urban heat islands. In H. J. S. Fernando (Ed.), Handbook of Environmental Fluid Dynamics, Volume Two. CRC Press/Taylor & Francis Group, LLC.

[18] Fathian, F., Prasad, A. D., Dehghan, Z., & Eslamian, S. (2015). Influence of land use/land cover change on land surface temperature using RS and GIS techniques. International Journal of Hydrology Science and Technology, 5(3), 195–207.

[19] Ullah, M., Li, J., & Wadood, B. (2020). Analysis of urban expansion and its impacts on land surface temperature and vegetation using RS and GIS: a case study in Xi'an City, China. Earth Systems and Environment, 4(3), 583–597.

[20] Ullah, S., Tahir, A. A., Akbar, T. A., Hassan, Q. K., Dewan, A., Khan, A. J., & Khan, M. (2019). Remote sensing-based quantification of the relationships between land use land cover changes and surface temperature over the lower Himalayan region. Sustainability, 11(19), 5492.

[21] Akbar, T. A., Hassan, Q. K., Ishaq, S., Batool, M., Butt, H. J., & Jabbar, H. (2019). Investigative spatial distribution and modelling of existing and future urban land changes and its impact on urbanization and economy. Remote Sensing, 11(2), 105.

[22] Khawaldah, H. A., Farhan, I., & Alzboun, N. M. (2020). Simulation and prediction of land use and land cover change using GIS, remote sensing and CA–Markov model. Global Journal of Environmental Science and Management, 6(2), 215–232.

[23] Mansour, S., Al-Belushi, M., & Al-Awadhi, T. (2020). Monitoring land use and land cover changes in the mountainous cities of Oman using GIS and CA–Markov modelling techniques. Land Use Policy, 91, 104414.

[24] Hadi, S. J., Shafri, H. Z., & Mahir, M. D. (2014). Modelling LULC for the period 2010–2030 using GIS and remote sensing: a case study of Tikrit, Iraq. IOP Conference Series: Earth and Environmental Science, 20(1), 012053.

[25] Artis, D. A., & Carnahan, W. H. (1982). Survey of emissivity variability in thermography of urban areas. Remote Sensing of Environment, 12(4), 313–329.

[26] Zhang, J., Wang, Y., & Li, Y. (2006). A C++ program for retrieving land surface temperature from the data of Landsat TM/ETM+ band 6. Computers & Geosciences, 32(10), 1796–1805.

[27] Becker, F., & Li, Z. L. (1995). Surface temperature and emissivity at various scales: definition, measurement and related problems. Remote Sensing Reviews, 12(3–4), 225–253.

[28] Prata, A., Caselles, V., Coll, C., Sobrino, J., & Ottle, C. (1995). Thermal remote sensing of land surface temperature from satellites: current status and future prospects. Remote Sensing Reviews, 12(3–4), 175–224.

[29] Weng, Q., Lu, D., & Schubring, J. (2004). Estimation of land surface temperature–vegetation abundance relationship for urban heat island studies. Remote Sensing of Environment, 89(4), 467–483.

[30] Sobrino, J. A., Jimenez-Muñoz, J. C., & Paolini, L. (2004). Land surface temperature retrieval from LANDSAT TM 5. Remote Sensing of Environment, 90(4), 434–440.

[31] Rizvi, S. H., Fatima, H., Iqbal, M. J., & Alam, K. (2020). The effect of urbanization on the intensification of SUHIs: analysis by LULC on Karachi. Journal of Atmospheric and Solar-Terrestrial Physics, 207, 105374.

[32] Liu, M., & Tian, H. (2010). China's land cover and land use change from 1700 to 2005: estimations from high-resolution satellite data and historical archives. Global Biogeochemical Cycles, 24(3).

[33] Mishra, V. N., & Rai, P. K. (2016). A remote sensing aided multi-layer perceptron–Markov chain analysis for land use and land cover change prediction in Patna district (Bihar), India. Arabian Journal of Geosciences, 9(4), 1–18.

[34] Hassan, M. M., & Nazem, M. N. I. (2016). Examination of land use/land cover changes, urban growth dynamics, and environmental sustainability in Chittagong City, Bangladesh. Environment, Development and Sustainability, 18(3), 697–716.

[35] Weng, Q. (2001). A remote sensing–GIS evaluation of urban expansion and its impact on surface temperature in Zhujiang Delta, China. International Journal of Remote Sensing, 22(10), 1999–2014.

[36] Li, Z.-L., Tang, B.-H., Wu, H., Ren, H., Yan, G., Wan, Z., Trigo, I. F., & Sobrino, J. A. (2013). Satellite-derived land surface temperature: current status and perspectives. Remote Sensing of Environment, 131, 14–37.

[37] Olorunfemi, J. F. (1983). Monitoring urban land use in developing countries—an aerial photographic approach. Environment International, 9(1), 27–32.

[38] Lillesand, T., Kiefer, R. W., & Chipman, J. (2015). Remote Sensing and Image Interpretation. John Wiley & Sons.

[39] Herold, M., Goldstein, N. C., & Clarke, K. C. (2003). The spatiotemporal form of urban growth: measurement, analysis and modeling. Remote Sensing of Environment, 86(3), 286–302.

[40] Verburg, P. H., Van De Steeg, J., Veldkamp, A., & Willemen, L. (2009). From land cover change to land function dynamics: a major challenge to improve land characterization. Journal of Environmental Management, 90(3), 1327–1335.